IEEE Access
Multidisciplinary ⋮ Rapid Review ⋮ Open Access Journal

Received March 21, 2021, accepted March 30, 2021, date of publication April 20, 2021, date of current version April 29, 2021.

Digital Object Identifier 10.1109/ACCESS.2021.3074322

A Legged Robot With Thigh Bi-Articular Muscle-Tendon Complex

SHUMA HIASA[1], (Member, IEEE), RYUKI SATO[1], (Member, IEEE), KANAKO KUROKAWA[1], LEI WANG[2,3], HUAXIN LIU[2,3], (Member, IEEE), FEI MENG[2,3], AND AIGUO MING[1], (Member, IEEE)

[1]Department of Mechanical Engineering and Intelligent Systems, Graduate School of Informatics and Engineering, The University of Electro-Communications, Chofu 182-8585, Japan
[2]Beijing Advanced Innovation Center for Intelligent Robots and Systems, Beijing Institute of Technology, Beijing 100081, China
[3]School of Mechatronical Engineering, Beijing Institute of Technology, Beijing 100081, China

Corresponding author: Shuma Hiasa (s_hiasa@mail.uec.jp)

ABSTRACT Recently, the development of agile-legged robots that mimic the structures and functions of biological muscles and tendons of quadruped mammals has attracted significant attention. The driving force of muscles and the elastic force of muscles and tendons can help improve the performances of these robots. Thus far, most of these robots have been developed based on the muscle-tendon complex of the lower legs. However, some mammals have a larger muscle-tendon complex on the upper legs, which contributes significantly to agile movements. In this study, a legged robot that mimics the functions of the bi-articular muscle-tendon complex of the thigh was developed, and its effects on static and dynamic movements were verified through simulations and experiments. While maintaining a static posture, the transfer of torque between two joints in the thigh mechanism reduced the power consumption by the robot's motors by half, used for balancing the gravity of the robot. For a dynamic vertical jump, the motion trajectory generation for the robot was performed using non-linear optimization to maximize the jump height. As a result, the jump height was significantly enhanced by the effect of the thigh mechanism, and the height was more than twice the leg length.

INDEX TERMS Bi-articular muscle-tendon complex, biomimetics, jump movement, legged robot, motion control.

I. INTRODUCTION

Among the quadruped mammals, felines particularly enable agile performances. For example, a cheetah is the fastest mammal on land and is known to run at a maximum speed of 29 m/s [1]. Similarly, a cat can jump over a large obstacle with a run-up that combines speed and agility. These performances by the animals are achieved through the effective utilization of the muscles and tendons [2], [3]. Moreover, the animals dynamically adjust the tensions of multiple muscles to provide an optimal output [4]. It is considered that applying a tensegrity mechanism to a legged robot can optimize the structural dimensions, mechanical strength, mass distribution, and energy consumption of the legs. Therefore, agile-legged robots that mimic the structure and functions of biological muscles and tendons have been developed worldwide.

To enable various motions, robots need to exhibit delicate controllability. Hence, the number of legged robots using electromagnetic motors with good controllability has been increasing year by year [5]–[9]. The MIT Cheetah [10]–[13] has a leg mechanism that delivers a low reduction ratio and high back-drivability, as it is equipped with high torque density electromagnetic motors. This enables it to jump over obstacles and perform different gaits, such as trotting, bouncing, and galloping. This research has realized the driving function of the muscles through the effective use of the motors. However, it does not realize the elastic elements of the muscles and tendons of mammals. The Cheetah-cub [14], [15], which is a small robot with a leg mechanism that mimics that of a mammal, has an elastic element and realizes an efficient trot gait. However, the leg extension is only passively performed by the elastic element; thus, it is not

The associate editor coordinating the review of this manuscript and approving it for publication was Luigi Biagiotti.

suitable for dynamic movements, such as jumping and fast running.

Among the one-legged robots that have elastic elements that mimic the structure of the muscles and tendons of mammals, some robots have an elastic mechanism that extends the knee joint to enhance performance. In [16], the robot has both series-elastic actuation (SEA) and parallel-elastic actuation (PEA) mimicking the tendons between the two joints of the knee and ankle. Although the mechanisms are sufficiently effective in consuming electrical energy in static motion, their effectiveness in dynamic motion has not yet been demonstrated. In addition, legged robots with elastic elements in the lower limb have been studied in [17] and [18]. The effectiveness of robots with elastic elements has been shown by verification in dynamic motions, such as jumping and vertical falling. However, their movements are not optimized and the elastic elements may not be fully utilized.

In our laboratory, research is being conducted to apply the functions of both muscles and tendons for dynamic motions to develop a more agile robot. Focusing on the musculoskeletal structure of feline mammals that move instantaneously, a leg ''Sugoi-Neco Legs'' that mimics the muscle-tendon complex between the knee and ankle joints was developed [19]. In mammals, the muscle-tendon complex is composed of the gastrocnemius muscle, which is a bi-articular muscle, and the achilles tendon. This complex acts cooperatively on the knee flexion and ankle extension and contributes to shock absorption at landing and kicking during jumping and running. The Sugoi-Neco Legs has a four-bar closed-link mechanism, which is termed as the elastic four-bar linkage mechanism (EFLM) between the knee and ankle joints. The elastic link enables the transfer of torque between the two joints as well as the storage and reuse of elastic energy. A small quadruped robot ''Sugoi-Neco'' equipped with the leg mechanism has realized stable running at 3.5 km/h and jumping forward by one body length [20].

In addition to the muscle-tendon complex between the knee and ankle joints, a muscle-tendon complex in the thigh of mammals is known to contribute significantly to dynamic performances. The thigh muscle-tendon complex is significantly large in the upper leg [1]. This complex acts on the hip flexion and knee extension. Because a large torque is required for extending the knee joint both for maintaining the posture in the stance phase and for kicking on the ground in dynamic motions, both static and dynamic performances of a legged robot may be improved by introducing the thigh muscle-tendon complex.

In this study, a mechanism that mimics the functions of the thigh muscle-tendon complex is introduced in a legged robot to enhance its performances during both the static and dynamic movements. It has been verified that the thigh mechanism, which is different from the EFLM developed in our previous study, reduces the power consumption by maintaining the posture and improves the ability to jump by increasing the torque to extend the knee joint.

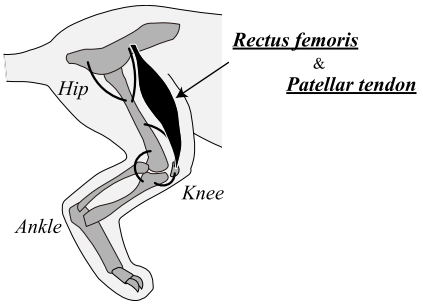

FIGURE 1. Mammal's hindlimb.

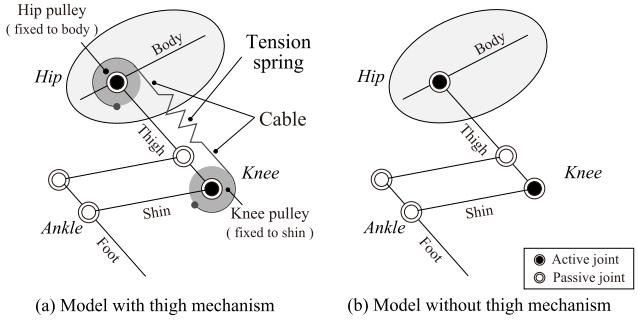

FIGURE 2. Schematic diagrams of legged mechanisms with and without the function of the thigh bi-articular muscle-tendon complex.

The rest of this paper is organized as follows. In Section II, the functions and contributions of the biological thigh muscle-tendon complex are described, and a mechanism that mimics this complex is proposed. Subsequently, the details of the prototype of the legged robot with the proposed mechanism are presented. In Section III, the effect of the static motion of the leg with the thigh mechanism is verified. The contribution of the thigh mechanism to weight compensation is indicated by the results of the statics calculation and experiment. In Section IV, motion generation of the legged robot is demonstrated to achieve a higher jump height by utilizing the thigh mechanism based on non-linear optimization. Through simulation, it is shown that this mechanism can contribute to enhancing the jump height. The contribution of this mechanism is also verified through experiments. Section V concludes the results and future research directions.

II. LEGGED ROBOT WITH BI-ARTICULAR MUSCLE-TENDON COMPLEX

A. MUSCULOSKELETAL STRUCTURES OF QUADRUPED MAMMAL

As shown in Fig. 1, there exists a significantly large bi-articular muscle-tendon complex in the thigh of the felidae. The muscle-tendon complex is composed of a bi-articular muscle called the rectus femoris and tendons attached to the ends of the muscle. The rectus femoris enables the transfer of torque between the hip and knee joints, and acts on the hip flexion and knee extension. Moreover, the muscle-tendon complex can store and reuse elastic energy using its elasticity.

B. LEG MECHANISM WITH THIGH BI-ARTICULAR MUSCLE-TENDON COMPLEX

Fig. 2 shows the schematic diagrams of legged mechanisms with and without the function of the thigh bi-articular muscle-tendon complex. The driving function of the rectus femoris is realized by a mechanism using cables and circular pulleys between the hip and knee joints. This enables the transfer of torque between the two joints. Moreover, a tension spring placed between the cables helps store and reuse elastic energy, such as the elasticity of muscles and tendons. When the spring is stretched, the torque due to the elastic force is transferred to each joint. Therefore, it can contribute to the hip flexion and knee extension.

The spring extension Δl is expressed as (1).

$$\Delta l = r_1(\theta_{10} - \theta_1) + r_2(\theta_2 - \theta_{20}) \tag{1}$$

where r_1 and r_2 are the pulleys' radii of the hip and knee joints. θ_1 and θ_2 are the angles of each joint, and θ_{10} and θ_{20} express the joint angles when the tension spring has a natural length. If the length is shorter than the natural length, the cable sags and the spring does not generate an elastic force. Therefore, the elastic force f_s and elastic energy U_s are expressed by (2) and (3), respectively.

$$f_s = \begin{cases} k\Delta l + f_{pre} & (\Delta l \geq 0) \\ 0 & (\Delta l < 0) \end{cases} \tag{2}$$

$$U_s = \begin{cases} \dfrac{1}{2}(k\Delta l + 2f_{pre})\Delta l & (\Delta l \geq 0) \\ 0 & (\Delta l < 0) \end{cases} \tag{3}$$

where k and f_{pre} represent the spring constant and pretension of the spring, respectively. The cable tension is always applied in the tangential direction of the pulleys at each joint, enabling the transfer of torque to each joint efficiently. Therefore, the torque of the hip and knee joints obtained by multiplying the elastic force with the pulleys' radii is applied to each joint. The torque due to the elastic force is expressed by (4) and (5).

$$\tau_{s1} = -f_s r_1 \tag{4}$$

$$\tau_{s2} = f_s r_2 \tag{5}$$

Next, we discuss the difference between the proposed thigh mechanism and the EFLM developed in our previous research [19], [20]. The thigh mechanism is located in the upper leg, whereas the EFLM is located in the lower leg. Both mechanisms enable the storage and reuse of elastic energy; however, EFLM can only use the spring passively. In contrast, the spring in the thigh mechanism can be used both actively and passively. Another advantage of the thigh mechanism is that efficient torque transmission is enabled with the use of pulleys.

C. LEGGED ROBOT

Fig. 3(a) shows a legged robot with the thigh muscle-tendon complex fabricated by authors. The height of the robot was 235 mm at the maximum extension of the knee joint, and its weight was 1103 g. The ranges of motion of the hip and knee joints were $-110° \leq \theta_1 \leq 102°$ and $39° \leq \theta_2 \leq 129°$. The hip and knee joints were actively driven by a brushless DC motor Parker K044050-8Y and a planetary gear reducer with a reduction ratio of 5 to realize the high back-drivability of the leg. To achieve agile movements, they were arranged coaxially to reduce the moment of inertia around the hip joint. Furthermore, the leg could transfer the torque of the knee joint's actuator to the ankle joint by introducing a parallel link mechanism between the two joints. Therefore, it was not necessary to mount an actuator on the ankle joint, thus reducing the weight of the leg.

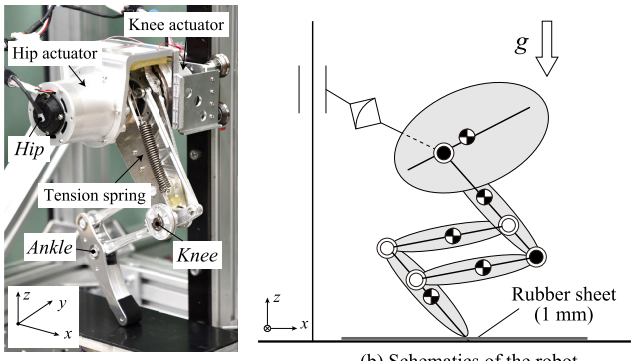

(a) Prototype of the robot

(b) Schematics of the robot
(The thigh mechanism is omitted)

FIGURE 3. Legged robot with thigh bi-articular muscle-tendon complex.

The tension spring that mimics the function of the thigh muscle-tendon complex was selected because it can be installed on the robot and exhibits relatively high rigidity. The spring constant was 2.1 N/mm. The torque transmission ratio was determined by the ratio of the pulleys' radii of the hip and knee joints; in this case, the ratio was set to 1:1 for simplification and the radii were designed to be $r_1 = r_2 = 13.5$ mm. At the natural length of the tension spring, the hip and knee joint angles were set to $\theta_{10} = 32.5°$ and $\theta_{20} = 39.0°$, respectively.

As shown in Fig. 3(b), the robot was attached to a linear guide fixed vertically to the ground, and the degree of freedom was restricted to the vertical translation and rotation around the Y-axis at the hip joint. Rubber sheets (thickness 1 mm) were attached to the toe and ground to reduce the slip.

III. STATIC EFFECT OF THIGH MUSCLE-TENDON COMPLEX

First, the effect of the leg with the thigh muscle-tendon complex was verified for maintaining a static posture during the stance phase. To maintain the posture of the leg, the joint motors need to output the torque to obtain a balance with the weight. In particular, the knee joint constantly requires torque in the extension direction, resulting in continuous power consumption. Because the thigh muscle-tendon complex can output the force in the direction of assisting the knee joint, it is necessary to investigate its effect on the power consumption due to the torque assist.

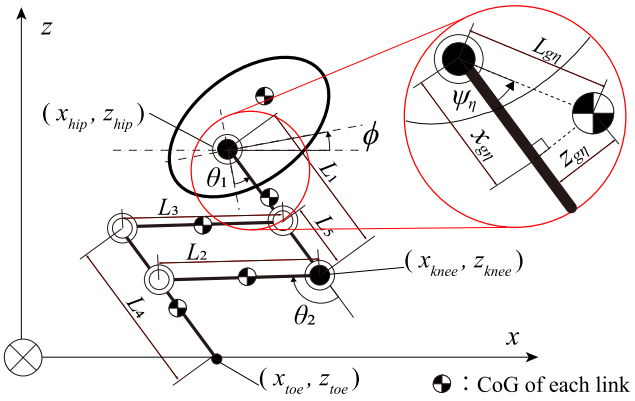

FIGURE 4. Model in the sagittal plane.

A. KINEMATICS

Fig. 4 shows the model in the sagittal plane. The elastic mechanism of the thigh was omitted. In the model, all the link lengths and the inertia of the robot were considered. In Fig. 4, L_η is the length, I_η is the moment of inertia about the center of gravity, and m_η is the mass of each link. ϕ is the body angle, $\boldsymbol{p}_\eta = (x_\eta, z_\eta)$ are the coordinates of the center of gravity (CoG) of each link in the global coordinate system, and (x_{joint}, z_{joint}) are the coordinates of each joint in the global coordinates. The parameters of the model were calculated from a prototype (3D–CAD) model of the robot and are shown in Table 1. The weight included the jig weight for the linear guide used in the experiment. Because the tension spring and the cables had a sufficiently small mass in comparison with the mass of the link, the influence of these masses was ignored.

The coordinates of the model's CoG $\boldsymbol{p}_G = (x_G, z_G)$ in the global coordinates are expressed by (6).

$$\boldsymbol{p}_G = \frac{\sum_{\eta=0}^{4} m_\eta \boldsymbol{p}_\eta}{\sum_{\eta=0}^{4} m_\eta} \tag{6}$$

Then, the coordinates of the body's CoG $\boldsymbol{p}_0 = (x_0, z_0)$ in the global coordinates are expressed as (7).

$$\boldsymbol{p}_0 = \boldsymbol{p}_G + \frac{1}{m_0} \sum_{\eta=1}^{4} m_\eta (\boldsymbol{p}_G - \boldsymbol{p}_\eta) \tag{7}$$

The distance $L_{g\eta}$ from the coordinates of the proximal joint to the coordinates of the CoG and the rotational angle ψ_η from the link axis of each link are expressed by (8) and (9), respectively.

$$L_{g\eta} = \sqrt{x_{g\eta}^2 + z_{g\eta}^2} \tag{8}$$

$$\psi_\eta = \arctan\left(\frac{z_{g\eta}}{x_{g\eta}}\right) \tag{9}$$

where $(x_{g\eta}, z_{g\eta})$ represents the relative coordinate of the CoG of each link to the proximal joint. Therefore, the kinematics can be solved using (7)–(9) and joint angles, and the coordinates of each joint in the global coordinates are calculated as (10)–(13).

TABLE 1. Parameters of the model.

Link	η	L_η [mm]	$(x_{g\eta}, z_{g\eta})$ [mm]	m_η [g]	I_η [kg · m^2]
Body	0	-	(0.00700, 4.30)	616	3.84×10^{-4}
Thigh	1	100	(4.90, 7.98)	404	3.65×10^{-4}
Shin	2	90	(-17.3, -0.320)	36.4	4.14×10^{-5}
RL	3	90	(-39.9, 0)	11.9	1.68×10^{-5}
Foot	4	88	(12.2, -1.19)	30.9	2.28×10^{-5}

$$\boldsymbol{p}_{hip} = \boldsymbol{p}_0 + \begin{pmatrix} -L_{g0}\cos(\phi + \psi_0) \\ -L_{g0}\sin(\phi + \psi_0) \end{pmatrix} \tag{10}$$

$$\boldsymbol{p}_{knee} = \boldsymbol{p}_{hip} + \begin{pmatrix} L_1 \sin(\phi + \theta_1) \\ -L_1 \cos(\phi + \theta_1) \end{pmatrix} \tag{11}$$

$$\boldsymbol{p}_{ankle} = \boldsymbol{p}_{knee} + \begin{pmatrix} L_2 \sin(\phi + \theta_1 - \theta_2) \\ -L_2 \cos(\phi + \theta_1 - \theta_2) \end{pmatrix} \tag{12}$$

$$\boldsymbol{p}_{toe} = \boldsymbol{p}_{ankle} + \begin{pmatrix} (L_4 - L_5)\sin(\phi + \theta_1) \\ -(L_4 - L_5)\cos(\phi + \theta_1) \end{pmatrix} \tag{13}$$

The coordinates of CoG of each link in the global coordinates are also obtained using (14)–(17).

$$\boldsymbol{p}_1 = \boldsymbol{p}_{hip} + \begin{pmatrix} L_{g1}\sin(\phi + \theta_1 + \psi_1) \\ -L_{g1}\cos(\phi + \theta_1 + \psi_1) \end{pmatrix} \tag{14}$$

$$\boldsymbol{p}_2 = \boldsymbol{p}_{knee} + \begin{pmatrix} L_{g2}\sin(\phi + \theta_1 - \theta_2 + \psi_2) \\ -L_{g2}\cos(\phi + \theta_1 - \theta_2 + \psi_2) \end{pmatrix} \tag{15}$$

$$\boldsymbol{p}_3 = \boldsymbol{p}_{hip} + \begin{pmatrix} (L_1 - L_5)\sin(\phi + \theta_1) \\ +L_{g3}\sin(\phi + \theta_1 - \theta_2 + \psi_3) \\ -(L_1 - L_5)\cos(\phi + \theta_1) \\ -L_{g3}\cos(\phi + \theta_1 - \theta_2 + \psi_3) \end{pmatrix} \tag{16}$$

$$\boldsymbol{p}_4 = \boldsymbol{p}_{ankle} + \begin{pmatrix} L_{g4}\sin(\phi + \theta_1 + \psi_4) \\ -L_{g4}\cos(\phi + \theta_1 + \psi_4) \end{pmatrix} \tag{17}$$

B. MOTOR POWER CONSUMPTION

The motor power consumption P_c is expressed as (18) during static motion. Note that the same motors were used for the hip and knee joints.

$$P_c = \sum_{i=1}^{2} {i_{Mi}}^2 R \tag{18}$$

where i_{Mi} is the current through each joint motor and R is the internal resistance. The motor torque τ_{Mi} is expressed as $\tau_{Mi} = K_T i_{Mi}$ using the current and the torque constant K_T. Subsequently, (19) can be obtained by substituting $i_{Mi} = \tau_{Mi}/K_T$ into (18).

$$P_c = \frac{R}{{K_T}^2} \sum_{i=1}^{2} {\tau_{Mi}}^2 \tag{19}$$

From the equation, it can be observed that the torque has a squared effect on power consumption. Therefore, the power consumption can be reduced by decreasing the torque required to maintain a static posture. In this calculation, the internal resistance was determined as $R = 1.787\ \Omega$

and the torque constant as $K_T = 0.04$ Nm/A with reference to the catalog value of the motor.

In the leg model with the thigh mechanism, the static relationship between the torque of the hip and knee joints $\boldsymbol{\tau}_A = \begin{bmatrix} \tau_{a1} & \tau_{a2} \end{bmatrix}^{\mathrm{T}}$ and the ground reaction force $\boldsymbol{f} = \begin{bmatrix} f_x & f_z \end{bmatrix}^{\mathrm{T}}$ is expressed as (20).

$$\boldsymbol{\tau}_A = -\boldsymbol{J}^{\mathrm{T}}\boldsymbol{f} + \begin{pmatrix} \tau_{s1} \\ \tau_{s2} \end{pmatrix} \tag{20}$$

where $\boldsymbol{J}$ is the jacobian $\boldsymbol{J} = \begin{bmatrix} \frac{\partial x_{toe}}{\partial \theta_1} & \frac{\partial x_{toe}}{\partial \theta_2}, & \frac{\partial z_{toe}}{\partial \theta_1} & \frac{\partial z_{toe}}{\partial \theta_2} \end{bmatrix}$ at the toe to the CoG of the model. In the static posture, when the CoG of the model is vertically above the toe, the horizontal ground reaction force f_x becomes 0. In addition, the vertical ground reaction force f_z is equal to the magnitude of gravity due to its own weight; therefore, $f_z = \sum_{\eta=0}^{4} m_\eta g$. g is the gravitational acceleration.

To verify the effect of the thigh muscle-tendon complex, the power consumptions in the cases with and without the mechanism were compared. In the model without the mechanism, the relationship between the torque of each joint $\boldsymbol{\tau}_B = \begin{bmatrix} \tau_{b1} & \tau_{b2} \end{bmatrix}^{\mathrm{T}}$ and the ground reaction force is expressed as (21).

$$\boldsymbol{\tau}_B = -\boldsymbol{J}^{\mathrm{T}}\boldsymbol{f} \tag{21}$$

Therefore, the power consumption of each model was calculated using the motor torque obtained by dividing (20) and (21) by the reduction ratio, as shown in (22) and (23).

$$P_{cA} = \frac{R}{\gamma^2 {K_T}^2} {\boldsymbol{\tau}_A}^{\mathrm{T}} \boldsymbol{\tau}_A \tag{22}$$

$$P_{cB} = \frac{R}{\gamma^2 {K_T}^2} {\boldsymbol{\tau}_B}^{\mathrm{T}} \boldsymbol{\tau}_B \tag{23}$$

where γ is the reduction ratio of the joint actuator.

In the verification, the power consumption was calculated in the posture from the flexed state to the extended state, and the difference between the cases with and without the thigh muscle-tendon complex was studied. The toe was placed just below the hip joint, and the knee joint angle was changed by 1° in the motion range. The hip joint angle was adjusted so that the body's angle to the ground was $\phi = 0°$.

C. SIMULATION RESULT OF POWER CONSUMPTION

Fig. 5 shows the total power consumption for the two cases. The power consumption was reduced by mounting the thigh muscle-tendon complex in any verified posture, with a maximum reduction of 48%. Fig. 6 shows the comparison of the required torque for each joint's motor in the two cases. Part of the load torque of the knee joint was distributed to the hip joint by mounting the thigh muscle-tendon complex, and the torque required by the knee joint's motor could be reduced. Therefore, it was confirmed that the thigh muscle-tendon complex has the ability to transfer the torque between the hip and knee joints, and that the total power consumption of the motors can be reduced by utilizing the effect of the muscle-tendon complex in maintaining a static posture.

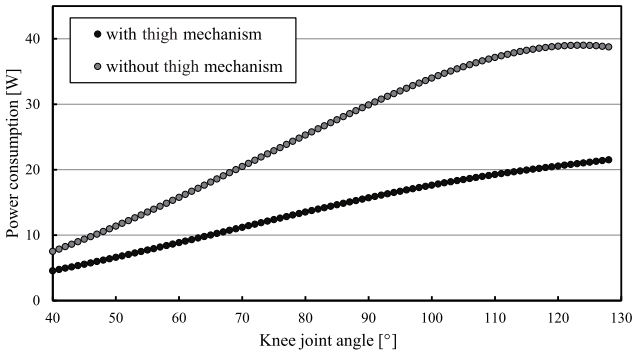

FIGURE 5. Power consumption.

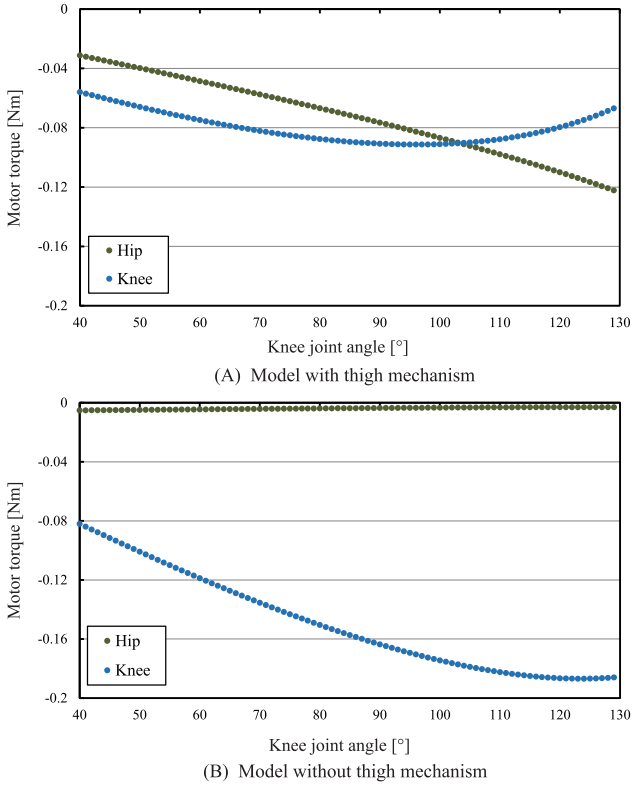

FIGURE 6. Motor torque.

The difference in the power consumption between the cases with and without the thigh mechanism is expressed by (24).

$$P_{cA} - P_{cB} = \frac{R}{{K_T}^2 \gamma^2} ({\boldsymbol{\tau}_A}^{\mathrm{T}} \boldsymbol{\tau}_A - {\boldsymbol{\tau}_B}^{\mathrm{T}} \boldsymbol{\tau}_B) \tag{24}$$

The amount of reduction in the power consumption is determined by the difference in the sum of squares of the joint torque of each model. From (20) and (21), (25) can be derived.

$${\boldsymbol{\tau}_A}^{\mathrm{T}} \boldsymbol{\tau}_A - {\boldsymbol{\tau}_B}^{\mathrm{T}} \boldsymbol{\tau}_B = 2 f_s (-r_1 \tau_{b1} + r_2 \tau_{b2}) + {f_s}^2 ({r_1}^2 + {r_2}^2) \tag{25}$$

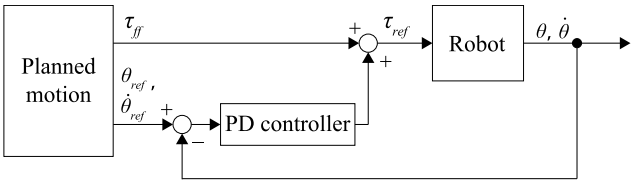

FIGURE 7. Block diagram of the robot controller.

The power consumption can be reduced by the effect of the thigh mechanism by varying the spring constant, pretension, and pulleys' radii such that (25) yields a negative value.

D. EXPERIMENT AND RESULTS

A demonstration experiment was conducted to confirm the effect of the thigh muscle-tendon complex on the reduction in the total power consumption shown by the calculation in Section III-C. The movement of the robot was limited to the translational motion in the vertical direction and the rotational motion around the Y-axis. The robot moved from a flexed posture to an extended posture. The robot was maintained in a posture for 5 s, and the joint angles and consumed currents for the last 1 s were collected and averaged for evaluation.

The block diagram of the control system is shown in Fig. 7. The torque obtained by dividing (20) and (21) by the reduction ratio was considered as the feedforward torque, and the torque due to PD control of the position using the feedback from the joint encoder was transferred as the feedback torque to each joint motor, as shown in (26).

$$\tau_{i,ref} = \tau_{i,ff} + K_p(\theta_{i,ref} - \theta_i) + K_d(\dot{\theta}_{i,ref} - \dot{\theta}_i) \quad (26)$$

where i is the joint index ($i = 1, 2$), and K_p and K_d are the proportional and derivative gains, respectively. θ_i and $\dot{\theta}_i$ are the angle and angular velocity of each joint, respectively. The target angles were the joint angles in each posture used in the calculation, and the target velocities were 0. The feedback control was operated with a sampling time of 2 ms. The experiment was performed 10 times for the robots with and without the thigh mechanism.

The results are shown in Fig. 8. The results were evaluated as an average of 10 trials. Error bars represent the standard deviation. It can be seen from Fig. 8(a) that the target posture could be achieved by both robots.

As can be seen from Fig. 8(b), the total power consumption could be reduced at any posture as in the calculation result, and the experimental value was almost in agreement with the calculated value. Then, by comparing the torque of the motors of each joint shown in Fig. 8(c), it was determined that almost all the torque required to maintain the posture was generated in the knee joint in the robot without the thigh mechanism. In contrast, the torque of the knee joint could be reduced by transferring a part of the torque required to maintain the posture to the hip joint using the function of torque transfer in the robot with the mechanism. As a result, the total power consumption was reduced as in the calculation result. Therefore, it can be concluded that the power consumption can be reduced by the thigh mechanism for a real robot.

IV. DYNAMIC EFFECT OF THIGH MUSCLE-TENDON COMPLEX

Based on the results presented in Section III, the large muscle-tendon complex was found to be effective in maintaining a static posture. In this section, the dynamic effect of the thigh muscle-tendon complex is investigated by considering the jumping movement.

As an example of motion generation aiming at the maximum jump, there exists a method of exploratively determining the optimum motion as an optimization problem. In [9], the jump height was maximized by optimizing the time variation of the ground reaction force during the jump in a serial two-link robot. For the trajectory generation, a simplified model wherein the mass of the robot is concentrated at one point of the body was used; however, the effect of the inertia of each link cannot be ignored in a dynamic motion, such as a vertical jump. Moreover, when a passive element, such as a spring, is used in the robot, the dynamics of each link cannot be ignored because the dynamic behavior of the robot is dependent on the dynamics of those elements significantly.

In this study, a dynamic model that is as close as possible to the real environment was developed based on the 3D-CAD model. As the dynamic model of the robot, a multi-body model was used, wherein each link contained information regarding the mass, position of the CoG, and moment of inertia. The contact with the ground, collision between the links at the limit of the range of motion, and dynamics of the actuators were considered in the model.

A. DERIVATION OF EQUATION OF MOTION

The equation of motion was derived using Lagrange's method. Lagrangian L is represented by the total kinetic energy K and the total potential energy U of the model and given as (27).

$$\begin{aligned} L &= K - U \\ &= \sum_{\eta=0}^{4} \frac{1}{2}\{m_\eta(\dot{x}_\eta^2 + \dot{z}_\eta^2) + I_\eta \delta_\eta^2\} - (\sum_{\eta=0}^{4} m_\eta g z_\eta + U_s) \end{aligned} \quad (27)$$

where δ_η represents the angular velocity of each link.

Therefore, the equation of motion was derived as (28) using the Lagrange method.

$$\boldsymbol{M}(\boldsymbol{q})\ddot{\boldsymbol{q}} + \boldsymbol{H}(\boldsymbol{q}, \dot{\boldsymbol{q}}) + \boldsymbol{G}(\boldsymbol{q}) = \boldsymbol{\tau} + \boldsymbol{E}^{\mathrm{T}}\boldsymbol{f} \quad (28)$$

where $\boldsymbol{q} \in \mathbb{R}^{5\times1}$ is the generalized coordinate $\boldsymbol{q} = [x_G, z_G, \phi, \theta_1, \theta_2]^{\mathrm{T}}$, $\boldsymbol{M}(\boldsymbol{q}) \in \mathbb{R}^{5\times5}$ is the inertia matrix, $\boldsymbol{H}(\boldsymbol{q}, \dot{\boldsymbol{q}}) \in \mathbb{R}^{5\times1}$ is the centrifugal force and Coriolis force, $\boldsymbol{G}(\boldsymbol{q}) \in \mathbb{R}^{5\times1}$ is the potential term, and $\boldsymbol{\tau} \in \mathbb{R}^{5\times1}$ is the joint torque input by the actuator $\boldsymbol{\tau} = [0, 0, 0, \tau_1, \tau_2]^{\mathrm{T}}$. $\boldsymbol{E}^{\mathrm{T}}\boldsymbol{f}$ represents the constraint of the model, $\boldsymbol{f}$ is the external force exerted by the environment, and $\boldsymbol{E}$ is the Jacobian at the position where the force is given.

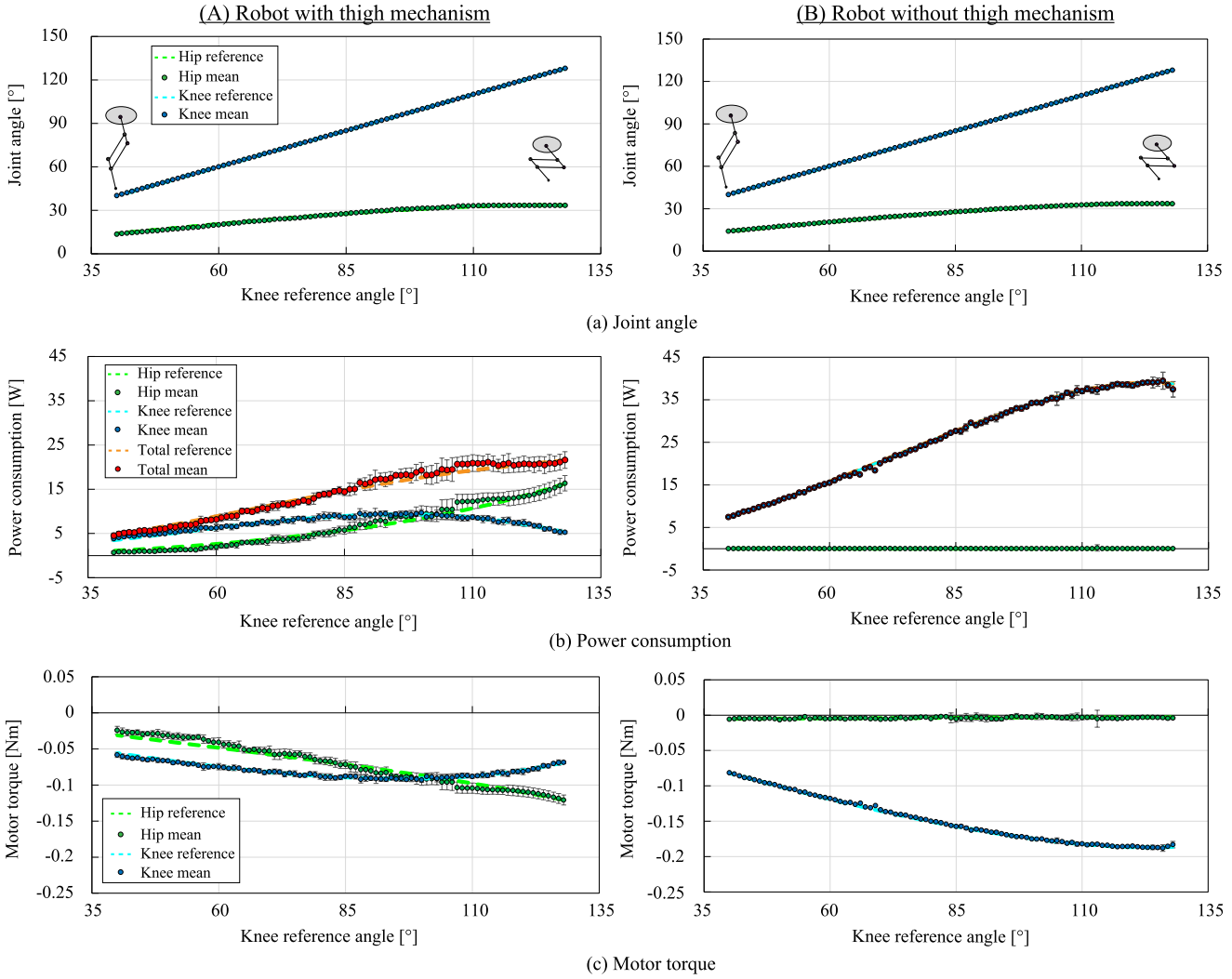

FIGURE 8. Experimental results of posture maintenance.

As the external force applied to the model, the constraint force from the guide f_{guide} required to maintain the horizontal position of the hip joint is constantly applied by the guide during the jump. Moreover, the ground reaction force f_x, f_z applied between the ground and toe is applied during the stance phase. Therefore, $\boldsymbol{E}$ and $\boldsymbol{f}$ are expressed as (29) and (30).

$$\boldsymbol{E} = \begin{cases} [\dfrac{\partial x_{toe}}{\partial \boldsymbol{q}}, \dfrac{\partial z_{toe}}{\partial \boldsymbol{q}}, \dfrac{\partial x_{hip}}{\partial \boldsymbol{q}}]^{\mathrm{T}} & \text{(stance phase)}, \\ \dfrac{\partial x_{hip}}{\partial \boldsymbol{q}} & \text{(free-fly phase)}. \end{cases} \tag{29}$$

$$\boldsymbol{f} = \begin{cases} [f_x, f_z, f_{guide}]^{\mathrm{T}} & \text{(stance phase)}, \\ f_{guide} & \text{(free-fly phase)}. \end{cases} \tag{30}$$

where x_{toe}, z_{toe}, and x_{hip} are the coordinates of the toe and hip joint, which are shown in Fig. 4 and can be calculated from (13) and (10).

A reaction torque was set at the limit of joint movement to consider the contact characteristics of the joint stop. This is expressed by (31) and can be modeled by adding it to the joint torque $\boldsymbol{\tau}$ of the equation of motion (28).

$$\begin{aligned} \tau_{r,i} &= \begin{cases} {k_{p,i}\epsilon_{i,m}}^{1.2} - k_{d,i}\dot{\theta}_i & (\theta_i < \theta_{i,min} \cap \dot{\theta}_i < 0) \\ {k_{p,i}\epsilon_{i,m}}^{1.2} & (\theta_i < \theta_{i,min} \cap \dot{\theta}_i \geq 0) \\ 0 & (\theta_{i,min} \leq \theta_i \leq \theta_{i,max}) \\ -{k_{p,i}\epsilon_{i,M}}^{1.2} & (\theta_i > \theta_{i,max} \cap \dot{\theta}_i < 0) \\ -{k_{p,i}\epsilon_{i,M}}^{1.2} - k_{d,i}\dot{\theta}_i & (\theta_i > \theta_{i,max} \cap \dot{\theta}_i \geq 0) \end{cases} \\ \epsilon_{i,m} &= -\theta_i + \theta_{i,min} \\ \epsilon_{i,M} &= \theta_i - \theta_{i,max} \end{aligned} \tag{31}$$

where $\theta_{i,min}$ and $\theta_{i,max}$ are the minimum and maximum angles of each joint, respectively. $k_{p,i}$ and $k_{d,i}$ are the coefficients related to the angle and angular velocity, respectively, and are determined to ensure that the behavior of the model does not

TABLE 2. Coefficients for the reaction torque.

Joint	$k_{p,i}$ [Nm/rad$^{1.2}$]	$k_{d,i}$ [Nms/rad]
θ_1 (hip)	100	0.5
θ_2 (knee)	100	5

considerably differ from that of the robot. The values for each joint are shown in Table 2.

B. FORWARD DYNAMICS

As shown in Fig. 3(b), the hip joint x coordinate of the robot x_{hip} does not move in the horizontal direction and the toe coordinate (x_{toe}, z_{toe}) does not move with respect to the ground during the stance phase. It is assumed that the toe does not slip during the stance phase. Therefore, if the constrained positions are set as $\boldsymbol{X} = [x_{toe}, z_{toe}, x_{hip}]^{\mathrm{T}}$, $d\boldsymbol{X}/dt = \boldsymbol{E}\dot{\boldsymbol{q}} = 0$ holds. Differentiating the equation with respect to time yields (32).

$$\dot{\boldsymbol{E}}\dot{\boldsymbol{q}} + \boldsymbol{E}\ddot{\boldsymbol{q}} = 0 \tag{32}$$

Therefore, if (28) and (32) are coupled simultaneously to solve the forward dynamics, the force $\boldsymbol{f}$ and the acceleration $\ddot{\boldsymbol{q}}$ are obtained as (33) and (34), respectively.

$$\boldsymbol{f} = -(\boldsymbol{E}\boldsymbol{M}^{-1}\boldsymbol{E}^{\mathrm{T}})^{-1}\{(\boldsymbol{E}\boldsymbol{M}^{-1}(\boldsymbol{\tau} - \boldsymbol{H} - \boldsymbol{G}) + \dot{\boldsymbol{E}}\dot{\boldsymbol{q}}\} \tag{33}$$

$$\ddot{\boldsymbol{q}} = \{\boldsymbol{M}^{-1} - \boldsymbol{M}^{-1}\boldsymbol{E}^{\mathrm{T}}(\boldsymbol{E}\boldsymbol{M}^{-1}\boldsymbol{E}^{\mathrm{T}})^{-1}\boldsymbol{E}\boldsymbol{M}^{-1}\} \times(\boldsymbol{\tau} - \boldsymbol{H} - \boldsymbol{G}) - \boldsymbol{M}^{-1}\boldsymbol{E}^{\mathrm{T}}(\boldsymbol{E}\boldsymbol{M}^{-1}\boldsymbol{E}^{\mathrm{T}})^{-1}\dot{\boldsymbol{E}}\dot{\boldsymbol{q}} \tag{34}$$

The robot's motion can be described by defining the joint torque $\boldsymbol{\tau}$ using (33) and (34).

C. MOTION TRAJECTORY GENERATION METHOD USING NON-LINEAR OPTIMIZATION

To determine the motion that maximizes the performance of the robot from the infinite motion trajectories, the motion trajectory was generated using the non-linear optimization simulation. Fig. 9 shows the simulation flow of the trajectory generation method.

The variation in the torque with time was parameterized using a B-spline curve, and the motion trajectory was generated using the optimization function. The motion trajectory was uniquely determined by inputting the torque as a variable into the equation of motion and calculating the forward dynamics as shown in Section IV-B. The torque's trajectory of each joint was defined by the B-spline curve, as shown in (35) [21].

$$\tau_i(t, \boldsymbol{P}_i) = \sum_{j=0}^{N} p_{i,j} B_{j,n+1}(t) \tag{35}$$

Equation (35) represents the B-spline curve of degree n. $\boldsymbol{P}_i$ is a control point vector composed of $N + 1 (N \geq n)$ elements $p_j (j = 0, 1, \cdots, N)$ of joint i, $t \in [t_n, t_N]$ is an element of a knot vector that defines a B-spline basis function, and $B(t)$ is the basis function. In the case of $n+1 > 1$, the basis function

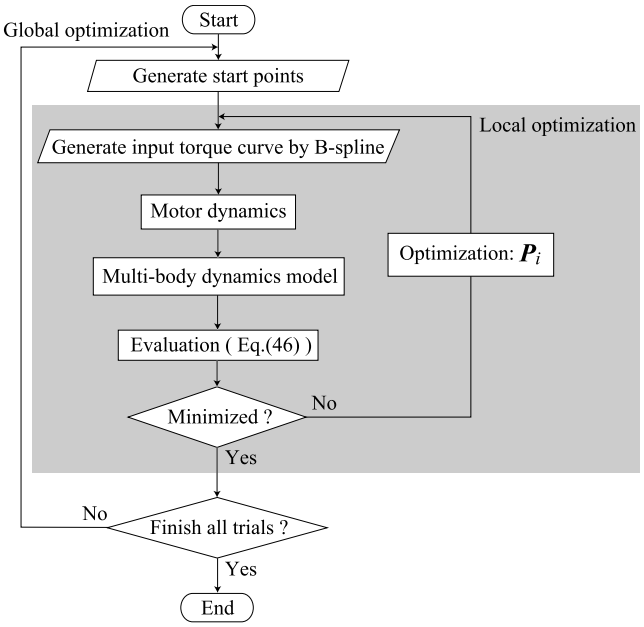

FIGURE 9. Optimization method.

is expressed as (36).

$$B_{k,n+1}(t) = \frac{t - t_k}{t_{k+n} - t_k} B_{k,n}(t) + \frac{t_{k+n+1} - t}{t_{k+n+1} - t_{k+1}} B_{k+1,n}(t) \tag{36}$$

Among the $n + N + 2$ elements of the knot vector, n elements at both ends were duplicated and the other elements were defined to increase at equal intervals as shown by (37) and (38). This was performed to plot an open uniform B-spline curve that matches the start and end points of the curve with the elements of the control point vector p_0 and p_N.

$$t := [t_0, t_1, \cdots, t_n, t_{n+1}, \cdots, t_N, t_{N+1}, \cdots, t_{N+n}, t_{N+n+1}] \tag{37}$$

$$t_k = \begin{cases} 0 & (k \leq n), \\ 1 & (k \geq N+1), \\ \dfrac{k-n}{N-n} & \text{otherwise.} \end{cases} \tag{38}$$

The joint torque required for the robot to maintain its initial posture was assigned to the first element p_0 of the control point vector. Therefore, the trajectories of the torque could be generated by arbitrarily defining the control point vector $\boldsymbol{P}_i$. In this study, $n = 3$ and $N = 13$ were determined, and the control point vectors for each joint were parameterized.

The knot vectors represented by (37) and (38) correspond to the normalized time axes of the trajectories, and we multiplied them by the control time ($T_{control} = 0.6$ s) which was determined to make the robot perform the agile movement. In addition, the B-spline curve is characterized by a function value that falls within the upper and lower limits of the control point when a non-decreasing knot vector is used. Therefore,

the maximum and minimum values of the control points were set as 80% of the stalling torque of the motor to secure the torque required for feedback control in the experiment. After defining a range constraint of $-\tau_{i,max} < \boldsymbol{P}_i < \tau_{i,max}$, $N - 2n + 1$ elements in $\boldsymbol{P}_i$ of each joint were used as the design variables. The motor model was used by defining the upper limit value τ_{ul} and lower limit value τ_{ll} of the torque according to the rotational speed, as shown in (39)–(41).

$$\tau_{ll} \leq \tau_M \leq \tau_{ul} \tag{39}$$

$$\tau_{ul} = \begin{cases} \tau_{M,max} & (\omega \leq \omega_s) \\ -\dfrac{K_T K_e}{R}\omega + \dfrac{K_T e}{R} & (\omega_s < \omega \leq \omega_n) \end{cases} \tag{40}$$

$$\tau_{ll} = \begin{cases} -\tau_{M,max} & (-\omega_s \leq \omega) \\ -(-\dfrac{K_T K_e}{R}\omega + \dfrac{K_T e}{R}) & (-\omega_n \leq \omega < -\omega_s) \end{cases} \tag{41}$$

τ_M is the torque of the motor, $\tau_{M,max}$ is the maximum torque of the motor, ω is the angular velocity of the motor, ω_s is the maximum angular velocity that can output the maximum torque, ω_n is the angular velocity at no load, e is the applied voltage, and K_e is the back electromotive force constant.

Based on the process shown in Fig. 9, a simulation program using MATLAB/Simulink was developed to generate the trajectory of the jump motion by the robot.

In the simulation, the model is initially in the stance phase at time $T = 0$. When the vertical ground reaction force is $f_z \geq 0$ N, the equation of motion in the stance phase is used for calculation. If the horizontal ground reaction force f_x does not satisfy (42) during the stance phase, toe slip occurs.

$$|f_x| \leq \mu f_z \tag{42}$$

where μ is the coefficient of the maximum static friction. The friction coefficient was determined as $\mu = 0.69$, which was measured between the robot's toe and the ground. Owing to the computational resolution in the simulation, (42) was not satisfied in the vicinity of $f_z = 0$, and the simulation could not proceed. Therefore, we decided to detect the slip of the toe only when $f_z \geq 5$ N. The trial was terminated when the slip of the toes occurred. The model was considered to take off when $f_z < 0$ N and the forward dynamics during the free-fly phase was calculated. Finally, the maximum jump height h_{max} was considered in the evaluation function.

Furthermore, the inclination angle was obtained with respect to the ground normal at the maximum height. Given $\boldsymbol{\alpha}_1 = (x_{hip} - x_{toe}, z_{hip} - z_{toe})$ and $\boldsymbol{\alpha}_2 = (0, 1)$, and considering the inner product of $\boldsymbol{\alpha}_1$ and $\boldsymbol{\alpha}_2$, (43) holds.

$$\cos\beta = \frac{\boldsymbol{\alpha}_1 \cdot \boldsymbol{\alpha}_2}{||\boldsymbol{\alpha}_1||\,||\boldsymbol{\alpha}_2||} \tag{43}$$

At this time, $\sin\beta$ is calculated by (44).

$$\sin\beta = \begin{cases} \sqrt{1 - \cos^2\beta} & (x_{hip} \leq x_{toe}) \\ -\sqrt{1 - \cos^2\beta} & (x_{hip} > x_{toe}) \end{cases} \tag{44}$$

TABLE 3. Maximum jump height and inclination angle in simulation.

Model	Jump height [mm]	Inclination angle [°]
Model A	584	-0.516
Model B	450	1.71

Therefore, the inclination angle at the highest point β was obtained from (45).

$$\beta = \arctan(\frac{\sin\beta}{\cos\beta}) \tag{45}$$

In this simulation, the *fmincon* function by MATLAB was adopted to obtain the minimum value of a non-linear multi-variable objective function and the interior point method was set as the optimization algorithm. In the optimization using the non-linear model, the optimization solution is highly dependent on the initial value. Therefore, a local optimization was performed with multiple initial values using the *MultiStart* function, which is the global optimization solver of MATLAB, and multiple local optimal solutions were searched globally. In this study, a global minimum solution was searched from 100,000 initial values. In the simulation, the solver ode45 on MATLAB was used, and the relative error was set to 0.001. The absolute error was set to be adjusted automatically with an upper bound of 0.001.

The optimization problem is expressed as (46).

$$\begin{aligned} &\min \quad F = w_1 f_h + w_2 f_\beta \\ &s.t.\ \boldsymbol{E}\dot{\boldsymbol{q}} = 0,\ |p_{i,k}| \leq \tau_{i,max}\ (k = 0, 1, \cdots, N),\ (39) \end{aligned} \tag{46}$$

where f_h and f_β are the normalized maximum jump height and inclination angle and are represented as $f_h = (1 - h_{max})/(1 - 0)$ and $f_\beta = \beta^2/(90^2 - 0^2)$, respectively. In addition to the maximum jump height, the inclination angle was also included in the evaluation function to obtain a motion trajectory that is easy to experiment with. w_1 and w_2 are the weights of the evaluation function and were set to $w_1 = 0.8$ and $w_2 = 0.2$. The initial posture was set to $\phi = 0°, \theta_1 = 28°$, and $\theta_2 = 85°$. To verify the effect of the thigh-muscle-tendon complex, the trajectory generation using the optimization calculation was performed for models with the mechanism (Model A) and without the mechanism (Model B).

D. SIMULATION RESULT

As a result of the motion generations, the maximum jump heights are shown in Table 3, and the motions are shown in Fig. 10. We observed that both models squatted once and then took-off. The squatting provides a large vertical acceleration at the CoG of the model before takeoff and increases the vertical extension speed at takeoff.

In Model A, which demonstrates the thigh mechanism, a higher jump motion was obtained. The height was approximately 2.5 times the leg length. In Model B in Fig. 11(a), the torque required to extend the knee joint reached the maximum torque of the actuator and was saturated before takeoff. In contrast, the torque of Model A was approximately 1 Nm

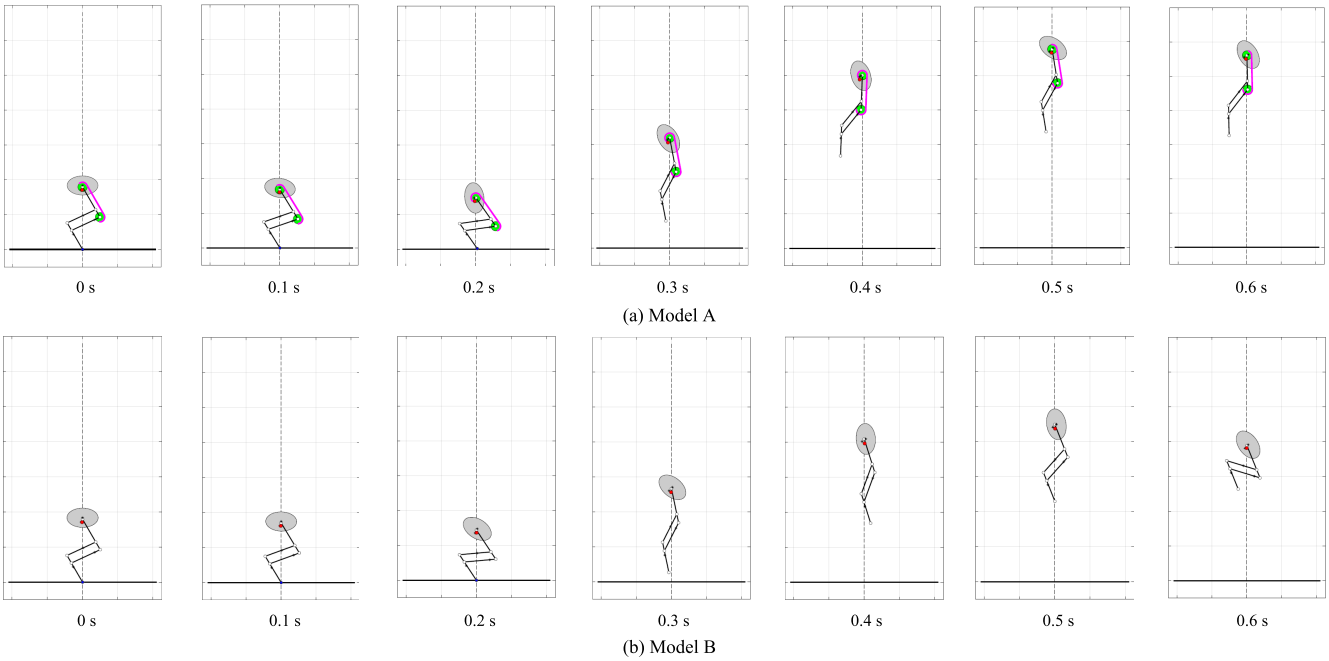

FIGURE 10. Generated vertical jump motions.

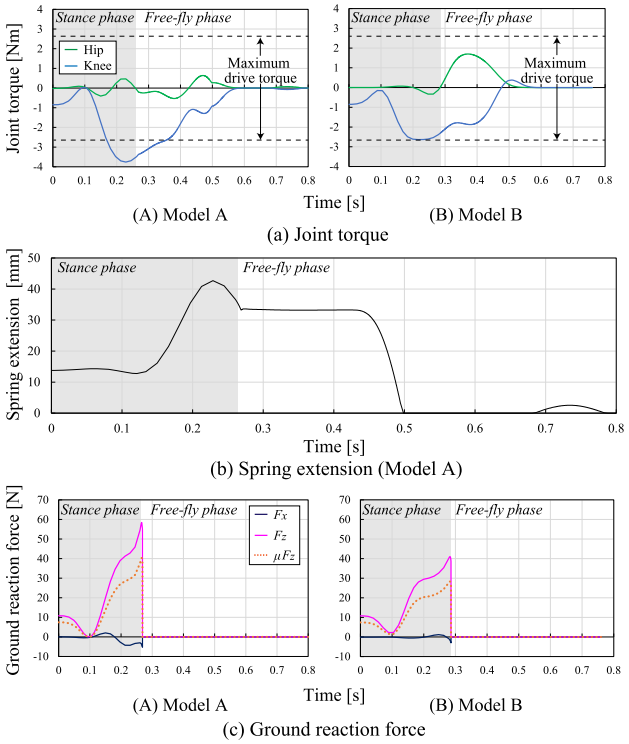

FIGURE 11. Simulation results.

greater than the maximum torque of the actuator. As can be seen from Fig. 11(b), the tension spring extends significantly from 0.15 s to 0.23 s. This is because a considerable amount of elastic energy is stored by extending the hip joint and further extending the tension spring during squatting, which can be utilized as the torque acting on the knee joint during extension. The torque that exceeds the maximum torque of the actuator acts on the knee joint because the torque of the hip joint is transferred to the knee joint. Therefore, it is considered that the vertical speed of the CoG increases due to the increased speed of extending the knee joint and the jump height is improved.

In Fig. 11(c), it can be seen that Model A can jump using a larger vertical ground reaction force f_z. This is because a larger torque could be generated in Model A to extend the knee joint. In terms of the slip of the toe, by comparing f_x and μf_z, we observe that there are very few instances wherein (42) is not satisfied in Model A. Therefore, it is considered that the slip detection using the threshold $f_z \geq 5$ N cuts off only a small part of the stance phase and the calculation using the threshold is suitable.

In addition, the difference in the energy in the initial state between Model A and Model B must be considered. In the initial state of Model A, the elastic energy of the tension spring had been already stored. The energy calculated using (3) is 0.199 J. If all this energy is converted into the potential energy of the CoG, jump height increased due to the elastic energy is 18.4 mm. Because the difference in jump heights between the two models is approximately 130 mm, it can be concluded that an optimal motion is obtained by utilizing the thigh mechanism in Model A. Therefore, it can be confirmed that the thigh mechanism is effective for dynamic motions, such as jumping.

E. VERTICAL JUMP EXPERIMENT

To confirm the effect of the thigh muscle-tendon complex in an actual environment based on the simulation result, the vertical jump experiment was conducted in the environ-

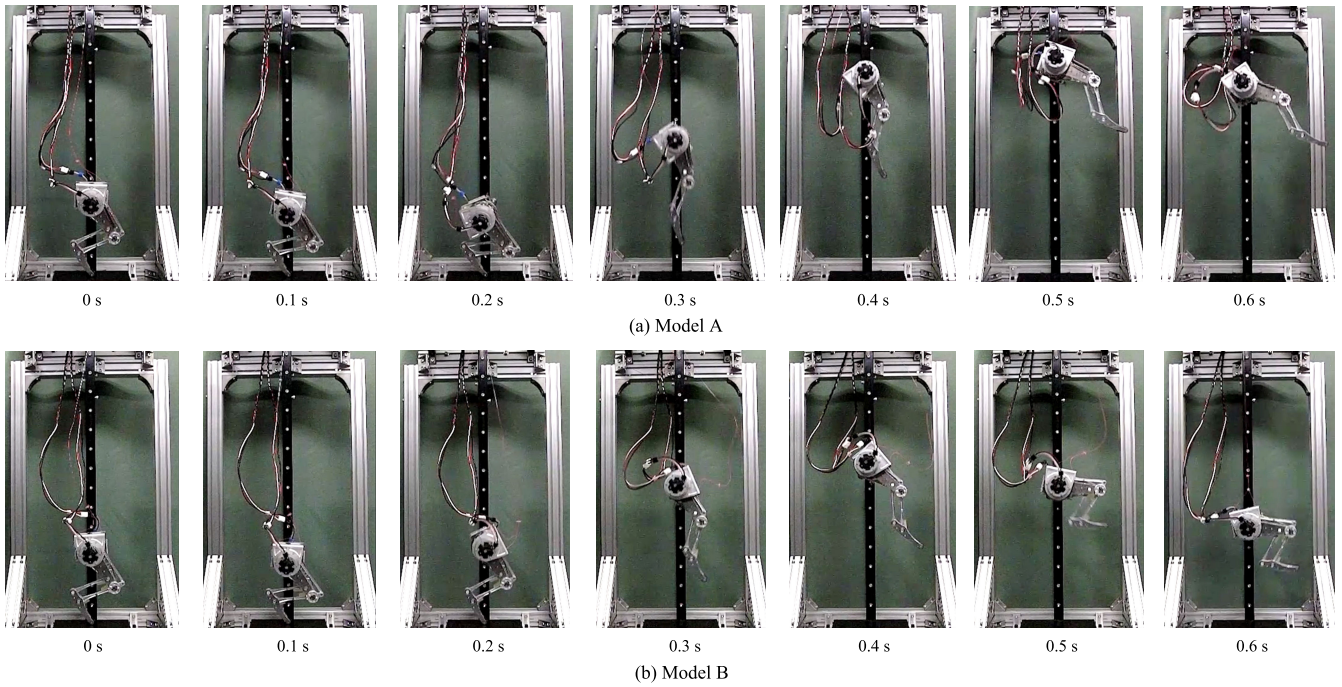

FIGURE 12. Vertical jump motion in the experiment.

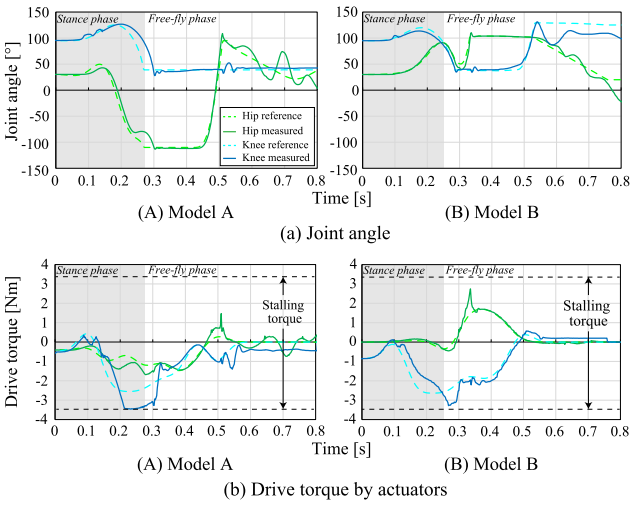

FIGURE 13. Experiment results.

ment, as shown in Fig. 3. The robot motion was limited to the translational motion in the vertical direction and the rotational motion around the Y-axis, as in the simulation. The same control system was used as in Section III-D. The trajectories of the angle and angular velocity obtained by the simulation were used as the target values $\theta_{i,ref}$ and $\dot{\theta}_{i,ref}$, respectively. The experiment was conducted for the models with and without the thigh mechanism as in the simulation.

As a result of the experiments, the maximum jump heights are shown in Table 4, and the motions are shown in Fig. 12. In Model A with the thigh mechanism, the jump height was more than twice the leg length. The slip of the toe was not observed in both models.

TABLE 4. Maximum jump height in the experiment.

Model	Jump height [mm]
Model A	550
Model B	419

The angle and drive torque of each joint are shown in Fig. 13. Position feedback torque was required to follow the target angle trajectory due to the influence of the weight of the wiring and the friction of the linear guide, which were not taken into consideration during the simulation. The stalling torque was obtained at the knee extension and it was not possible to generate the torque that could follow the target angle trajectory by the position feedback. Therefore, the jump height was lower than that in the simulation.

Model A with the thigh-muscle-tendon complex achieved a higher jump as in the simulation and its height was improved by approximately 31%. In the robot with the thigh muscle-tendon complex (Model A), the joint torque and spring extension calculated by (1) using the angles of the hip and knee joints are shown in Fig. 14. The joint torque is the sum of the drive torque shown in Fig. 13(b) and the torque generated by the thigh mechanism shown in (4) and (5). Comparing the torques of the knee joints in Fig. 13(b) and Fig. 14(a), although the motor reached the stalling torque in both models, the knee joint of Model A could exert an additional torque of approximately 1 Nm due to the thigh mechanism. Furthermore, as shown in Fig. 14(b), the spring

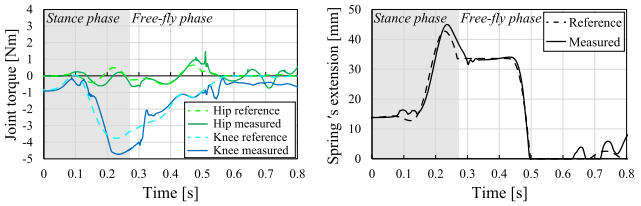

(a) Joint torque (b) Spring´s extension

FIGURE 14. **Joint torque and spring extension (Model A).**

could be significantly extended during the motion and the elastic energy could be stored as in the simulation. Therefore, it is considered that the jump height can be improved by utilizing the thigh muscle-tendon complex effectively.

V. CONCLUSION

This study aimed to enhance robot performance by introducing a mechanism that mimics the thigh bi-articular muscle-tendon complex of a mammal into a legged robot. The functions of the thigh muscle-tendon complex were simulated using cables, pulleys, and a tension spring between the hip and knee joints, and a legged robot with the mechanism was fabricated. The effect of the thigh mechanism on weight compensation was verified while maintaining a static posture. It was shown that the power consumption of the joint motors could be reduced by the transfer of torque between the hip and knee joints by the thigh mechanism. In addition, optimal motion generation for the legged robot was performed to maximize the jump height during a dynamic vertical jump. As a result, it was confirmed that the jump height was significantly improved by the thigh mechanism in the simulation and the experiment.

In the future, we intend to extend this research to a quadruped robot. We plan on realizing continuous jumping and running motions, further utilizing the thigh muscle-tendon complex. Moreover, because the biological muscle-tendon complex also contributes to a soft landing, we will continue to study motion control with the aim of achieving the soft landing by the robot.

REFERENCES

[1] R. M. Alexander, *Principles of Animal Locomotion*. Princeton, NJ, USA: Princeton Univ. Press, 2003.
[2] R. M. Alexander, *Elastic Mechanisms in Animal Movement*. Cambridge, U.K.: Cambridge Univ. Press, 1988.
[3] A. A. Biewener, *Animal Locomotion*. London, U.K.: Oxford Univ. Press, 2003.
[4] Y. Zhong, R. Wang, H. Feng, and Y. Chen, "Analysis and research of quadruped robot's legs: A comprehensive review," *Int. J. Adv. Robot. Syst.*, vol. 16, no. 3, pp. 1–15, 2019.
[5] M. Hutter, C. Gehring, D. Jud, A. Lauber, C. D. Bellicoso, V. Tsounis, J. Hwangbo, K. Bodie, P. Fankhauser, M. Bloesch, R. Diethelm, S. Bachmann, A. Melzer, and M. Hoepflinger, "ANYmal—A highly mobile and dynamic quadrupedal robot," in *Proc. IEEE/RSJ Int. Conf. Intell. Robots Syst. (IROS)*, Oct. 2016, pp. 38–44.
[6] M. Hutter, C. Gehring, M. A. Höpflinger, M. Blösch, and R. Siegwart, "Toward combining speed, efficiency, versatility, and robustness in an autonomous quadruped," *IEEE Trans. Robot.*, vol. 30, no. 6, pp. 1427–1440, Dec. 2014.
[7] G. Kenneally, A. De, and D. E. Koditschek, "Design principles for a family of direct-drive legged robots," *IEEE Robot. Autom. Lett.*, vol. 1, no. 2, pp. 900–907, Jul. 2016.
[8] Y. H. Lee, Y. H. Lee, H. Lee, L. T. Phan, H. Kang, Y. B. Kim, and H. R. Choi, "Development of torque controllable leg for running robot, AiDIN-IV," in *Proc. IEEE/RSJ Int. Conf. Intell. Robots Syst. (IROS)*, Sep. 2017, pp. 4125–4130.
[9] Y. Ding and H.-W. Park, "Design and experimental implementation of a quasi-direct-drive leg for optimized jumping," in *Proc. IEEE/RSJ Int. Conf. Intell. Robots Syst. (IROS)*, Sep. 2017, pp. 300–305.
[10] D. J. Hyun, J. Lee, S. Park, and S. Kim, "Implementation of trot-to-gallop transition and subsequent gallop on the MIT Cheetah I," *Int. J. Robot. Res.*, vol. 35, no. 13, pp. 1627–1650, Nov. 2016.
[11] P. M. Wensing, A. Wang, S. Seok, D. Otten, J. Lang, and S. Kim, "Proprioceptive actuator design in the MIT Cheetah: Impact mitigation and high-bandwidth physical interaction for dynamic legged robots," *IEEE Trans. Robot.*, vol. 33, no. 3, pp. 509–522, Jun. 2017.
[12] H.-W. Park, P. M. Wensing, and S. Kim, "High-speed bounding with the MIT Cheetah 2: Control design and experiments," *Int. J. Robot. Res.*, vol. 36, no. 2, pp. 167–192, Feb. 2017.
[13] H.-W. Park, S. Park, and S. Kim, "Variable-speed quadrupedal bounding using impulse planning: Untethered high-speed 3D running of MIT Cheetah 2," in *Proc. IEEE Int. Conf. Robot. Automat. (ICRA)*, May 2015, pp. 5163–5170.
[14] A. Spröwitz, A. Tuleu, M. Vespignani, M. Ajallooeian, E. Badri, and A. J. Ijspeert, "Towards dynamic trot gait locomotion: Design, control, and experiments with Cheetah-cub, a compliant quadruped robot," *Int. J. Robot. Res.*, vol. 32, no. 8, pp. 932–950, Jul. 2013.
[15] A. Spröwitz, M. Ajallooeian, A. Tuleu, and A. J. Ijspeert, "Kinematic primitives for walking and trotting gaits of a quadruped robot with compliant legs," *Frontiers Comput. Neurosci.*, vol. 8, p. 27, Mar. 2014.
[16] W. Roozing, Z. Ren, and N. G. Tsagarakis, "An efficient leg with series-parallel and biarticular compliant actuation: Design optimization, modeling, and control of the eLeg," *Int. J. Robot. Res.*, vol. 40, no. 1, pp. 1–17, 2019.
[17] X. Liu, A. Rossi, and I. Poulakakis, "A switchable parallel elastic actuator and its application to leg design for running robots," *IEEE/ASME Trans. Mechatronics*, vol. 23, no. 6, pp. 2681–2692, Dec. 2018.
[18] F. Ruppert and A. Badri-Spröwitz, "Series elastic behavior of biarticular muscle-tendon structure in a robotic leg," *Frontiers Neurorobotics*, vol. 13, p. 64, Aug. 2019.
[19] R. Sato, I. Miyamoto, K. Sato, A. Ming, and M. Shimojo, "Development of robot legs inspired by bi-articular muscle-tendon complex of cats," in *Proc. IEEE/RSJ Int. Conf. Intell. Robots Syst. (IROS)*, Sep. 2015, pp. 1552–1557.
[20] E. Kazama, R. Sato, I. Miyamoto, A. Ming, and M. Shimojo, "Development of a small quadruped robot with bi-articular muscle-tendon complex," in *Proc. IEEE Int. Conf. Robot. Biomimetics (ROBIO)*, Dec. 2015, pp. 1059–1064.
[21] R. F. Riesenfeld, "Applications of B-spline approximation to geometric problems of computer-aided design," Ph.D. dissertation, Dept. Elect. Eng. Comput. Sci., Univ. Syracuse, Syracuse, NY, USA, 1973.

SHUMA HIASA (Member, IEEE) received the B.S. and M.S. degrees in engineering from The University of Electro-Communications (UEC), Chofu, Japan, in 2017 and 2019, respectively. He has been working as an Engineer with Canon Inc., since 2019.

RYUKI SATO (Member, IEEE) received the B.Eng., M.Eng., and Ph.D. degrees in engineering from The University of Electro-Communications (UEC), Chofu, Japan, in 2014, 2016, and 2020, respectively. He was a Research Fellow with the Japan Society for the Promotion of Science (JSPS), from 2017 to 2019. He is currently a Postdoctoral Researcher with the Department of Mechanical and Intelligent Systems Engineering, UEC. His research interests include bio-inspired robotics, design and control of legged robots, and dynamic legged locomotion.

KANAKO KUROKAWA received the B.S. and M.S. degrees in engineering from The University of Electro-Communications (UEC), Chofu, Japan, in 2018 and 2020, respectively. She has been working as an Engineer with Sony Corporation, since 2020.

LEI WANG received the B.S. degree in electrical engineering and automation from Shenyang Jianzhu University, Shenyang, China, in 2013, and the M.S. degree in control science and engineering from the Beijing University of Civil Engineering and Architecture, Beijing, China, in 2016. He is currently pursuing the Ph.D. degree with the School of Mechatronical Engineering, Intelligent Robotics Institute, BIT, Beijing. His research interest includes quadruped robot dynamic locomotion.

HUAXIN LIU (Member, IEEE) received the B.Eng. degree from the Beijing University of Aeronautics and Astronautics (BUAA), in 2009, and the Ph.D. degree in engineering from the Beijing Institute of Technology (BIT), Beijing, China, in 2016. He was a Visiting Scholar with the Dynamic Legged Robotics Laboratory, Oregon State University, Corvallis, OR, USA, from 2013 to 2014. He was a Customer Researcher with the Ming Laboratory, The University of Electro-Communications (UEC), Chofu, Japan, from 2016 to 2018. He is currently a Researcher with the Beijing Advanced Innovation Center for Intelligent Robotics and Systems, BIT. His research interests include humanoid robots, design and system integration of legged robots, and dynamic legged locomotion.

FEI MENG received the B.S. and Ph.D. degrees in mechatronics engineering from the Beijing Institute of Technology (BIT), China, in 2008 and 2016, respectively. He was a Visiting Student with the Department of Mechanical Engineering and Intelligent Systems, The University of Electro-Communications, Japan, in 2015. He is currently a Postdoctoral Researcher with the School of Mechatronics Engineering, BIT.

AIGUO MING (Member, IEEE) received the Ph.D. degree in precision machinery engineering, The University of Tokyo, Japan, in 1990.

He is currently a Professor with the Department of Mechanical Engineering and Intelligent Systems, The University of Electro-Communications, Chofu, Japan. His current research interests include biomimetic hyper-dynamic robotics, soft robotics, intelligent robot hands, and precise measuring systems.